DESIGN AND FLIGHT TESTING OF A DIGITAL OPTIMAL CONTROL GENERAL AVIATION AUTOPILOT

J. R. Broussard
Information & Control Systems, Inc. (ICS)
28 Research Drive
Hampton, VA 23666

D. R. Downing
University of Kansas
Dept. of Aerospace Engineering
2004 Learned Hall
Lawrence, KS 66045

W. H. Bryant
NASA/Langley Research Center
Flight Control Systems Division
Hampton, VA 23665

ABSTRACT

This paper presents the designs of Proportional-Integral-Filter (PIF) autopilots for a General Aviation (NAVION) aircraft. The PIF autopilots use modern control theory to determine heading select and altitude select and hold autopilot modes. The PIF control law uses typical General Aviation sensors for state feedback; command error integration for command tracking; digital complimentary filtering and analog prefiltering for sensor noise suppression; a control filter for computation delay accommodation; and the incremental form to eliminate trim values in implementation. Theoretical developments for the control law are described which combine the sampled-data regulator with command generator tracking for use as a digital flight control system. The digital PIF autopilots are evaluated using closed-loop eigenvalues and simulations. Successful flight test results for the PIF autopilots are presented for different turbulence conditions and quadratic weights.

I. INTRODUCTION

Commercially available General Aviation (GA) autopilots are currently in transition from an analog circuit system to a state-of-the-art computer implemented digital flight control system[1]. Advantages of a digital autopilot include enhanced modes, self-test capability, fault detection, lower cost and greater computational capacity. A digital autopilot's computational capacity can be used to full advantage by increasing the sophistication of the digital autopilots chief function, stability and control. Direct digital design techniques along with proven computerized design and evaluation tools should be used to efficiently develop low-iteration rate advanced digital autopilots.

The General Aviation Terminal Area Operation Research (GATOR) program of the National Aeronautics and Space Administration is developing and evaluating advanced flight control and display concepts that make use of the recent advances in digital flight control theory, digital control hardware and electronic displays. The GATOR program uses the Princeton Avionics Research Aircraft[2] to flight test digital controllers programmed in the ROLM 1666 digital flight computer.

The purpose of this report is to present the development, design and flight test results of a proportional-integral-filter (PIF) digital autopilot design flown on the research aircraft. The PIF control law is a direct digital design operating at a low iteration rate (10 cycles per sec) that employs modern multivariable control theory to compute control gains. The PIF control law is specially structured to be designed using linear models but implemented to control and stabilize nonlinear aircraft dynamics. The PIF control law has features to accommodate computation delay, suppress high frequency noise and track commands using integral control. An earlier version of PIF has been investigated and successfully flight tested in the VALT autoland program [3],[4]. The new feature in this paper is the command model shown in Fig. 1, which is different for each autopilot mode.

II. AUTOPILOT SUMMARY

The General Aviation 3-axis PIF autopilot described in this paper combines recent developments in multivariable command generator tracking[5] and the sampled-data regulator[6] to design heading select and altitude select and hold autopilot modes. In the heading select mode, the pilot enters the desired heading, the autopilot command model commands the PIF control law to bank the aircraft, fly a coordinated turn in the shortest direction to the new heading, and roll the aircraft out of the turn to smoothly capture and hold the new heading. In the altitude select mode, the pilot enters the desired altitude and the autopilot command model commands the PIF control law to gradually ascend (or descend) the aircraft, establish a constant rate of climb (or descent) then smoothly capture and hold the new altitude. A number of other autopilot functions which are not discussed in this paper were also designed and successfully flight tested using the PIF approach[7]. These functions included roll select, pitch select and localizer/glideslope capture and track modes. The construction of the control tracking system is such that the other autopilot functions are simple variations of the altitude select and heading select modes both from a design (similar cost function weights) and implementation (similar software) viewpoint.

III. AIRCRAFT CHARACTERISTICS

Physical characteristics of the Princeton Avionics Research Aircraft (ARA) are similiar to a standard NAVION and are summarized in Table 1. The autopilot designs command elevator, ailerons and rudder using fly-by-wire control. The fast acting control surfaces are driven by hydralic servos

originally fitted to a B-58 aircraft. All autopilot control gains are determined at one flight condition using the estimated stability derivatives in Table 1[8]. Comparisons between the linear model and the aircraft response for individual step inputs in elevator and rudder are shown in Fig. 2. The longitudinal dynamics match is good while the lateral-directional match proved to be adequate; providing a good test of control system robustness.

IV. CONTROL LAW DEVELOPMENT

A derivation of the discrete-time PIF control structure is summarized in this section. Complete details are given in[7]. The perturbation state vector of the vehicle is augmented to contain the perturbation control and is driven by the control rate. Integral states are augmented to the state vector to operate on the error between aircraft states, $\Delta\underline{y}$, and a command model output, $\Delta\underline{y}_m$. Assuming that the control, $\Delta\underline{u}$, the control difference, $\Delta\underline{v}$, and the Euler implemented integrator state, $\Delta\underline{\xi}$, are constant over a sampling interval, Δt, the discrete plant representation becomes,

$$\begin{bmatrix}\Delta\underline{x}\\ \Delta\underline{u}\\ \Delta\underline{\xi}\end{bmatrix}_{k+1} = \begin{bmatrix}\Phi & \Gamma & 0\\ 0 & I & 0\\ \Delta tH & \Delta tD & I\end{bmatrix}\begin{bmatrix}\Delta\underline{x}\\ \Delta\underline{u}\\ \Delta\underline{\xi}\end{bmatrix}_k + \begin{bmatrix}0\\ \Delta tI\\ 0\end{bmatrix}\Delta\underline{v}_k \qquad (1)$$

Φ is the aircraft model state transition matrix and Γ is the control effect matrix. The matrices H and D determine the output as shown in (2) that is integrated to produce the control law's Type 1 property.

Actuator dynamics, prefilters and complementary filters are neglected in the construction of (1). A control computation time of one sampling interval is accommodated in the design. Control difference, used as the control variable, causes the control position command issued at time t_k to use state feedback information available at t_{k-1}. The sampling interval that transpires between receiving state information and releasing the actuator position command is used to update filter estimates, compute the actuator command, perform logic tests and any other side tasks. The states in (1) are determined by assuming a total state, $\underline{x}_k$ can be divided into nominal $\underline{x}_{o,k}$ and perturbation, $\Delta\underline{x}_k$, components. The perturbation component dynamics can be represented by a linear time-invariant system for small changes in $\underline{u}_k$.

The main objective of the PIF control is to cause

$$\Delta\underline{y}_k = H\Delta\underline{x}_k + D\Delta\underline{u}_k \qquad (2)$$

to optimally track the output of a linearized command model,

$$\Delta\underline{x}_{m,k+1} = \Phi_m\Delta\underline{x}_{m,k} + \Gamma_m\Delta\underline{u}_{m,k+1} \qquad (3)$$

$$\Delta\underline{y}_{m,k} = H_m\Delta\underline{x}_{m,k} + D_m\Delta\underline{u}_{m,k+1} \qquad (4)$$

In the derivation to follow, $\Delta\underline{u}_m$ is assumed to change once at t_o and remain constant thereafter. In implementation, the command model control input is not constant and the command model dynamics are nonlinear. When $\Delta\underline{u}_m$ is changing, $\Delta\underline{y}$ and $\Delta\underline{y}_m$ become mismatched and their error is governed by the closed-loop dynamics and the integrator. When $\Delta\underline{u}_m$ is constant, $\Delta\underline{y}$ eventually tracks $\Delta\underline{y}_m$ along the star trajectory, $\Delta\underline{x}^*$ and $\Delta\underline{u}^*$ (assuming no plant parameter variations). The star trajectory is discussed in[5] for continuous-time linear systems. The star trajectory is a linear system version of the nominal trajectory; a relationship that is exploited in (23).

The star trajectory for discrete-time systems with a constant command model input is determined from

$$\begin{bmatrix}\Delta\underline{x}^*_k\\ \Delta\underline{u}^*_k\end{bmatrix} = \begin{bmatrix}A_{11} & A_{12}\\ A_{21} & A_{22}\end{bmatrix}\begin{bmatrix}\Delta\underline{x}_{m,k}\\ \Delta\underline{u}_m\end{bmatrix} \qquad (5)$$

The feedforward matrices A_{ij} satisfy

$$\begin{bmatrix}(\Phi-I) & \Gamma\\ H & D\end{bmatrix}\begin{bmatrix}A_{11} & A_{12}\\ A_{21} & A_{22}\end{bmatrix} = \begin{bmatrix}A_{11}(\Phi_m-I) & A_{11}\Gamma_m\\ H_m & D_m\end{bmatrix} \qquad (6)$$

a solvable[9] matrix algebraic equation. The star trajectory is a convenient notational abstract and is not generated in implementation. The linear simulations in Section VI show the star trajectory for clarity.

The tracking objective of the control law is introduced into the design by defining the variables

$$\Delta\tilde{\underline{x}}_k = \Delta\underline{x}_k - \Delta\underline{x}^*_k \;; \quad \Delta\tilde{\underline{u}} = \Delta\underline{u}_k - \Delta\underline{u}^*_k \qquad (7a,b)$$

$$\Delta\tilde{\underline{v}}_k = \Delta\underline{v}_k - A_{21}(\Delta\underline{x}_{m,k+1} - \Delta\underline{x}_{m,k})/\Delta t \qquad (8)$$

$$\Delta\tilde{\underline{\xi}}_k = \Delta\underline{\xi}_k - \Delta\underline{\xi}^*_k \;; \quad \Delta\bar{\underline{x}}^T_k = \begin{bmatrix}\Delta\tilde{\underline{x}}^T_k & \Delta\tilde{\underline{u}}^T_k & \Delta\tilde{\underline{\xi}}^T_k\end{bmatrix} \qquad (9a,b)$$

and the discrete cost function,

$$J = \sum_{k=-1}^{\infty} \Delta\bar{\underline{x}}_k\,\hat{Q}\Delta\bar{\underline{x}}_k + 2\Delta\bar{\underline{x}}_k\,\hat{M}\Delta\tilde{\underline{v}}_k + \Delta\tilde{\underline{v}}_k\,\hat{R}\Delta\tilde{\underline{v}}_k \qquad (10)$$

The cost function weighting matrices are determined by first specifying a continuous cost function and converting to the equivalent discrete form which accounts for vehicle behavior between iterations[6]. The state vector $\Delta\bar{\underline{x}}_k$ satisfies a propagation equation using the transition and control effect matrices in (1), which are represented as $\bar{\Phi}$ and $\bar{\Gamma}$, respectively. The plant is assumed to be tracking the model for constant $\Delta\underline{u}_m$ previous to $t_o = 0$. The cost function starts at -1 since $\Delta\underline{u}_o$, and $\Delta\underline{\xi}^*_{-1}$ are to be determined. The quantities, $\Delta\underline{u}^*_{-1}$ and $\Delta\underline{x}^*_{-1}$ are defined in (5) using $\Delta\underline{u}_{m,o}$ instead of $\Delta\underline{u}_{m,-1}$. The standard use of the linear quadratic cost function is to regulate non-zero initial condition states to zero. The cost function in (10) is constructed so that the non-zero initial conditions in $\Delta\bar{\underline{x}}_{-1}$ are caused by the change in the command input at $t_o = 0$. The control law optimally transfers the system between star trajectories for a step change in $\underline{u}_m$. In practice, the control law performs well if $\underline{u}_m$ changes intermittently or "slowly" varies.

The control law which minimizes (10) is,

$$\Delta\tilde{v}_k = -(\hat{R} + \bar{\Gamma}^T P\bar{\Gamma})^{-1}(\bar{\Gamma}^T P\bar{\Phi} + \hat{M}^T)\,\Delta\bar{x}_k \tag{11}$$

where P is the steady-state solution of a discrete-time Riccati equation. The minimum value for J is,

$$J_{min} = \Delta\bar{x}_{-1}^T P\,\Delta\bar{x}_{-1} \tag{12}$$

Further minimizing J by setting $\partial J/\partial\Delta\tilde{\xi}_{-1} = 0$, because $\Delta\xi^*_{-1}$ is unspecified yields,

$$\Delta\xi^*_k = \begin{bmatrix}0 & A\end{bmatrix}\begin{bmatrix}\Delta x_{m,k}\\ \Delta u_{m,o}\end{bmatrix} = \Delta\xi^*_{-1} \tag{13}$$

$$A = -P_{\xi\xi}^{-1}\left[P_{x\xi}^T A_{12} + P_{u\xi}^T A_{22}\right] \tag{14}$$

The control law in (11) can be partitioned as

$$\Delta\tilde{v}_k = \begin{bmatrix}C_4 & C_5\end{bmatrix}\begin{bmatrix}\Delta\tilde{x}_k\\ \Delta\tilde{u}_k\end{bmatrix} + C_3\,\Delta\tilde{\xi}_k \tag{15}$$

and is determined using body-axes perturbation states for the aircraft model. The implementable control law must use sensor outputs for feedback,

$$\Delta z_k^T = [\Delta V, \Delta a_z, \Delta q, \Delta\theta, \Delta h_B, \Delta a_y, \Delta r, \Delta p, \Delta\phi, \Delta\psi] \tag{16}$$

The typical general aviation sensors instrumented on the aircraft are rate gyros (p, q, r), accelerometers (a_y, a_z), attitude gyro (ϕ, θ), heading gyro (ψ), airspeed (V) and a barometric altimeter (h_B). The barometric altimeter provides a noisy voltage output proportional to absolute height above sea level and is digitally complementary filtered with the normal accelerometer to smooth the height estimate ($\hat{h}_B$). The feedback gains in (15) are adjusted to use sensor output by computing the linear relationship between perturbation body-axis states and perturbation sensor output states,

$$\begin{bmatrix}\Delta\tilde{z}_k\\ \Delta\tilde{u}_k\end{bmatrix} = \begin{bmatrix}C_x & C_u\\ 0 & I\end{bmatrix}\begin{bmatrix}\Delta\tilde{x}_k\\ \Delta\tilde{u}_k\end{bmatrix} \tag{17}$$

The relationship in (17) is substituted into (15) as follows

$$\begin{bmatrix}C_4 & C_5\end{bmatrix}\begin{bmatrix}\Delta\tilde{x}_k\\ \Delta\tilde{u}_k\end{bmatrix} = \begin{bmatrix}C_4 & C_5\end{bmatrix}\begin{bmatrix}C_x & C_u\\ 0 & I\end{bmatrix}^{-1}\begin{bmatrix}\Delta\tilde{z}_k\\ \Delta\tilde{u}_k\end{bmatrix}$$

$$= \begin{bmatrix}C_1 & C_2\end{bmatrix}\begin{bmatrix}\Delta\tilde{z}_k\\ \Delta\tilde{u}_k\end{bmatrix} \tag{18}$$

The feedforward gains for the sensors are determined using (17) and (5) as follows,

$$\begin{bmatrix}\Delta z^*_k\\ \Delta u^*_k\end{bmatrix} = \begin{bmatrix}C_x & C_u\\ 0 & I\end{bmatrix}\begin{bmatrix}A_{11} & A_{12}\\ A_{21} & A_{22}\end{bmatrix}\begin{bmatrix}\Delta x_{m,k}\\ \Delta u_{m,o}\end{bmatrix}$$

$$= \begin{bmatrix}S_{11} & S_{12}\\ A_{21} & A_{22}\end{bmatrix}\begin{bmatrix}\Delta x_{m,k}\\ \Delta u_{m,o}\end{bmatrix} \tag{19}$$

After converting to sensor feedback, the control law is expressed in incremental form. The incremental form is obtained by subtracting $\Delta\tilde{v}_{k-2}$ from $\Delta\tilde{v}_{k-1}$ using (15),

$$\Delta\tilde{u}_k = \Delta\tilde{u}_{k-1} + \Delta t\,\Delta\tilde{v}_{k-1} \tag{20}$$

$$\Delta\tilde{v}_{k-1} = (I + \Delta t\,C_2)\Delta\tilde{v}_{k-2} + C_1(\Delta\tilde{z}_{k-1} - \Delta\tilde{z}_{k-2}) + C_3(\Delta\tilde{\xi}_{k-1} - \Delta\tilde{\xi}_{k-2}) \tag{21}$$

The perturbation variables and trim variables are eliminated from (20) and (21) using a large number of substitutions and cancellations. The implementable total value PIF equations reduce to the following

$$u_k = u_{k-1} + \Delta t\,v_{k-1} + A_{21}(x_{m,k} - x_{m,k-1}) \tag{22}$$

$$e_{k-1} = z_{k-1} - S_{11}\,x_{m,k-1} \tag{23}$$

$$v_{k-1} = (I + \Delta t\,C_2)\,v_{k-2} + C_1(e_{k-1} - e_{k-2}) + \Delta t\,C_3(y_{k-2} - y_{m,k-2}) + (-C_3A - C_1S_{12} - C_5A_{22})\,(u_{m,k} - u_{m,k-1}) \tag{24}$$

The gains which feedforward u_m are grouped together to minimize the multiplications and additions in implementation.

As an example of the steps used to obtain the implementable PIF equations, the sensor feedback increment simplification is detailed. Expanding the sensor feedback increment into total value and nominal states produces

$$\Delta\tilde{z}_{k-1} - \Delta\tilde{z}_{k-2} = (z_{k-1} - z_{k-2}) - (z_{o,k-1} - z_{o,k-2}) - S_{11}\left[(x_{m,k-1} - x_{m,k-2}) - (x_{mo,k-1} - x_{mo,k-2})\right] - S_{12}\left[(u_{m,k} - u_{m,k-1}) - (u_{mo} - u_{mo})\right] \tag{25}$$

For each increment, the change in the aircraft nominal state can be reasonably approximated by the corresponding incremental change in the nominal star trajectory. Using (19), the approximation at each time increment can be represented mathematically as

$$z_{o,k-1} - z_{o,k-2} \cong S_{11}\,(x_{mo,k-1} - x_{mo,k-2}) + S_{12}\,(u_{mo} - u_{mo}) \tag{26}$$

Substituting (26) into (25) and simplifying the result yields

$$\Delta\tilde{z}_{k-1} - \Delta\tilde{z}_{k-2} = (z_{k-1} - S_{11}x_{m,k-1}) - (z_{k-2} - S_{11}x_{m,k-2}) - S_{12}(u_{m,k} - u_{m,k-1}) \tag{27}$$

an equation which uses only computed and measured total values.

The index for $\underline{u}_m$ in (24) agrees with the control action that should occur at t_o. In the two autopilot designs in this paper, A_{21} is a zero matrix and S_{11} contains only zeroes and ones. A simplified block diagram of the control law is shown in Fig. 1.

V. COMMAND GENERATOR

Each autopilot mode uses a command model which is regulated by a nonlinear command model control system. When an autopilot mode is engaged, the internal states in the command model are initialized to the aircraft states. After initialization, the PIF control law follows state trajectories generated by the command model. When the command model receives a pilot command, the nonlinear command model control system maneuvers the command model to the new condition. The command model control system is designed simultaneously with the PIF feedback feedforward/gains to provide good ride quality and command limiting.

The heading select and hold command system (HDG SEL) performs the bank to turn autopilot feature. The HDG SEL command model uses the nonlinear kinematics which assume a coordinated turn, (10)

$$\psi_{m,k+1} = \psi_{m,k} + \Delta t \frac{g}{\hat{V}_k} \tan \phi_{m,k} \tag{28}$$

$$\phi_{m,k+1} = \phi_{m,k} + \Delta t \, \dot{\phi}_{m,k} \tag{29}$$

A digital low-pass filtered airspeed measurement is used for $\hat{V}_k$ in (28) and g is gravity. The command error used by the integrators in PIF is

$$\underline{y}_k - \underline{y}_{m,k} = \begin{bmatrix} \phi \\ \delta_r \end{bmatrix}_k - \begin{bmatrix} 1 & 0 \\ a_k & 1 \end{bmatrix} \begin{bmatrix} b\,(\psi_k - \psi_{m,k}) \\ \delta_{rm,k} \end{bmatrix} \tag{30}$$

A heading error multiplied by the constant gain, b, is used to command the aircraft bank angle (10). The trim rudder command from the model, δ_{rm}, is chosen to cause sideslip to be zero in straight and level flight. The rudder command can be preprogrammed or the measured value at engage can be used (the latter is used in flight test presented in Section VI). The roll command to rudder crossfeed gain, a_k, is used to provide a coordinated turn. The crossfeed gain is scheduled as a function of airspeed and computed using A_{22} in (5) for a $\left[\phi_m, \beta_m\right]$ constant command system.

The linear perturbation command model used in (3) and (4) for the HDG SEL autopilot mode is

$$\Delta\psi_{m,k+1} = \Delta\psi_{m,k} + \begin{bmatrix} \Delta t \; g/V_o & 0 \end{bmatrix} \begin{bmatrix} \Delta\phi_m \\ \Delta\delta_{rm} \end{bmatrix} \tag{31}$$

$$\Delta\underline{y}_{m,k} = \begin{bmatrix} -b \\ -a_o b \end{bmatrix} \Delta\psi_{m,k} + \begin{bmatrix} 0 & 0 \\ 0 & 1 \end{bmatrix} \begin{bmatrix} \Delta\phi_m \\ \Delta\delta_{rm} \end{bmatrix} \tag{32}$$

$$\Delta\underline{y}_k = \begin{bmatrix} \Delta\phi_k - b\,\Delta\psi_k \\ -a_o b\,\Delta\psi_k + \Delta\delta_{r,k} \end{bmatrix} \tag{33}$$

Equation 31 is obtained by linearizing the coordinated turn equation, (28), for the command model and neglecting velocity perturbations. Increasing the order of the linear perturbation command model to use $\Delta\dot{\phi}_m$ as the control variable proved to be unnecessary since satisfactory performance is obtained using ϕ_m.

The HDG SEL nonlinear command model control system uses $\dot{\phi}_{m,k}$ as the control variable. The command model control system causes $\psi_{m,k}$ to smoothly transfer from one pilot requested heading command, ψ_c, to another. The control system is

$$u_c = -b_1(\psi_{c,k} - \psi_{m,k}) - b_2\,\phi_{m,k} \tag{34}$$

$$\dot{\phi}_{m,k} = u_c \tag{35}$$

$$\text{IF } |\phi_{m,k}| \geq \phi_{max} \quad \text{THEN } \dot{\phi}_{m,k} = 0.0 \tag{36}$$

$$\text{IF } |\psi_{c,k} - \psi_{m,k}| \leq \psi_e \quad \text{THEN } \dot{\phi}_{m,k} = u_c \tag{37}$$

$$\text{IF } |\dot{\phi}_{m,k}| \geq \dot{\phi}_{max} \quad \text{THEN } \dot{\phi}_{m,k} = \text{SIGN}(\dot{\phi}_{m,k}) * \dot{\phi}_{max} \tag{38}$$

$$\text{IF } (\psi_{c,k} - \psi_{m,k}) * u_c < 0.0 \quad \text{THEN } \dot{\phi}_{m,k} = u_c \tag{39}$$

The value for $\dot{\phi}_{m,k}$ obtained after (39) is used to propagate (29). The control system banks the model up to the maximum bank angle, ϕ_{max}. The maximum bank angle can be adjusted using airspeed so that $\dot{\psi}$ is constant. If the yaw error is below the test value, ψ_e, the control system anticipates the roll back to zero before completing the turn so that the yaw angle overshoot of the aircraft is small.

The altitude select and hold (ALT SEL) command system allows the pilot to hold the current altitude or select a new altitude the aircraft should establish. When the pilot selects a new altitude, the autopilot smoothly accelerates (or decelerates) aircraft vertical speed into a constant rate of climb (or constant rate of descent) until the new altitude is approached, then captures and holds the aircraft at the selected altitude.

The altitude select command model is

$$\begin{bmatrix} z_{m,k+1} \\ \dot{z}_{m,k+1} \end{bmatrix} = \begin{bmatrix} 1 & \Delta t \\ 0 & 1 \end{bmatrix} \begin{bmatrix} z_{m,k} \\ \dot{z}_{m,k} \end{bmatrix} + \begin{bmatrix} 0 \\ \Delta t \end{bmatrix} \ddot{z}_{m,k} \tag{40}$$

$$y_k - y_{m,k} = z_k - z_{m,k} \tag{41}$$

The altitude acceleration, $\ddot{z}_{m,k}$, is used by the designer as a control variable to transfer z_m from one desired altitude, z_c, to another. The linear command model uses only the first row of (40) and treats $\dot{z}_m$ as the control variable. The ALT SEL command model control system has the same structure as (34) to (39) where ϕ_m, $\dot{\phi}_m$, ψ_m, ψ_c, ψ_e, ϕ_{max} and $\dot{\phi}_{max}$ are replaced with $\dot{z}_m$, $\ddot{z}_m$, z_m, z_c, z_e, $\dot{z}_{max}$, and $\ddot{z}_{max}$.

VI. DIGITAL CONTROL DESIGN AND FLIGHT TESTS

The airborne mechanization consisted of sensors, analog prefilters, two digital complementary filters, a command generator and a PIF controller. All sensors initially used analog prefilters designed with 0.01 sec time constants. These prefilters were used to eliminate potential aliasing in sampled signals. During flight tests, spurious oscillations in the sampled accelerometer outputs (traced to engine vibration) were observed, as shown in Fig. 3. The oscillations were suppressed by adjusting the analog prefilter time constant to 0.1 sec for the accelerometer sensors. The 0.1 sec time constant prefilters had little effect on lateral stability as shown in the 45 degree heading change flight test in Fig. 4.

Two digital complementary filters were included in the control design. One combined the barometric altimeter, vertical accelerometer, pitch attitude and roll attitude data to estimate altitude, rate of climb and accelerometer bias. The second complimentary filter combined yaw rate and heading to estimate heading and to smooth the heading gyro sensor output discontinuity that occurs as the sensor switched between ± 180 degrees.

The parameters in the ALT SEL and HDG SEL command generator control system shown in (34) to (39) were designed using simulations. The designs were adjusted until the command generators yielded smooth transition between pilot commands with no overshoot. The only parameter adjusted after the first flight test was the maximum vertical acceleration, $\ddot{z}_{max}$, which was decreased by a factor of 2. The design parameters for the command generator control systems are given in Table 2.

Three heading select autopilot design gain sets were developed using the NASA Langley Research Center computer facilities prior to flight testing; a baseline design (Table 3) and two alternatives. One alternative used higher quadratic weights on the states than the baseline design, while the other alternative used lower quadratic weights. All three designs gave good Dutch roll damping and spiral mode stability. Closed-loop eigenvalues for the baseline design are shown in Table 3. The HDG SEL autopilot feedback/feedforward gains for the baseline design are shown in Table 4.

All three designs yielded good simulation transient response. A quasi-linear simulation of the HDG SEL autopilot baseline design is shown in Fig. 5. The aircraft and control dynamics are linear, but the command model uses (34) to (39). The star trajectory from (5) is the dotted line in Fig. 5. The 45 degree change in heading begins with the autopilot command model banking the aircraft to the roll angle limit, executing a steady coordinated turn, then returning to wings level with no perceived heading angle overshoot.

A flight test for a 45 degree heading change is shown in Fig. 4 for light turbulance flight conditions. The linear simulation and flight test result have comparable good performance. The pilots judged the baseline design slightly superior to the alternatives and indicated that all three designs provided typical 3-axis state-of-the-art autopilot performance.

Figure 5 shows the baseline design HDG SEL autopilot executing a 45 degree heading change during heavy turbulence conditions. The pilot, with the autopilot engaged, reduced airspeed to values just above stall, then issued the command change. In both the HDG SEL and the ALT SEL autopilots, the pilot manually adjusted throttle to maintain the desired airspeed. The heading change was performed without difficulty. The ALT SEL autopilot was engaged during the maneuver to hold constant altitude during the turn. While not shown in Fig. 6, the ALT SEL autopilot exhibited adequate performance under these conditions.

As in the HDG SEL autopilot, three ALT SEL gain sets were designed prior to flight testing. The primary difference in the ALT SEL designs was the weighting on the height error integrator state, which mainly resulted in different height error integrator gains. Flight tests were performed and the pilots judged the middle design gain set as superior to the other two designs. The pilots indicated, however, that all three designs had a noticable altitude hunting oscillation.

Closed-loop eigenvalues for the middle design are shown in Table 3, (the low pitch weight design) and are well damped. The altitude complementary filter previously mentioned is not modeled in the control loop. Flight test results for a 157.4m (500 ft) altitude ascent are shown in Fig. 7. The altitude hunting is perceived to be caused by atmospheric disturbances perturbing the aircraft, causing the autopilot to interplay height and pitch attitude in an oscillatory (phugoid mode frequency) manner. Switching to radar altitude measurements in the altitude complementary filter did not improve the performance of the ALT SEL autopilot. Figure 8 shows the low pitch weight ALT SEL autopilot executing a 157.4m (500 ft) ascent during heavy turbulence conditions. The changes in turbulence with increasing height and its effect on the pitch oscillation is evident in the figure. Flight test results clearly illustrated problem areas in even the most preferred simulation based design. An effort was made to modify the ALT SEL autopilot design during flight testing operations.

The autopilots were implemented in a high level language (FORTRAN), operated in floating point arithmetic and could be modified easily using text editors. A computer aided autopilot design program[9] was used to compute control gains. The program uses the ORACLS subroutine package[11] to solve matrix equations encountered in modern control design problems. The autopilot tuning procedure involved using the computer-aided design program resident on the main NASA Langley Research Center computer complex, implementing the gain changes in the flight computer, and retesting the autopilot performance

in flight. Since flight operations were conducted at NASA's Wallops Flight Center, a remote terminal-modem connection to the Langley facility was utilized. This capability allowed many autopilot tuning iterations to be carried out within a few days at the flight test facility.

Design iterations were made focusing on penalizing pitch attitude deviations in the quadratic cost function. The improved ALT SEL design, whose closed-loop eigenvalues are shown in Table 3, has higher pitch weighting and a more damped elevator-pitch mode. The increase in damping is performed without significantly changing the height error integrator gain as shown in Table 4. The quasi-linear simulation for the improved ALT SEL autopilot is shown in Fig. 9 for a smooth 30.48m (100 ft) descent. The higher acceleration during the capture of the desired height is built into the command model. The pilots preferred the anticipatory cue that the autopilot was completing the maneuver. The speed mode time history in Fig. 9 is stable, but has a large time constant determined primarily by the aerodynamics[12]. Weighting Δu in the cost function degrades the altitude select function.

The design ALT SEL gain set 157.4m (500 ft) altitude ascent flight test is shown in Fig. 10. The pitch oscillations in Fig. 10 are more random in nature. The pilots perceived that the altitude hunting was eliminated when the higher pitch weight gain set was activated. The plane flew straight and level when holding constant altitude in light turbulence. The improved ALT SEL autopilot was judged by the pilots as comparable to a 3-axis state-of-the-art autopilot with the altitude select feature.

VII. CONCLUSIONS

A modern optimal digital flight control system has been designed for a General Aviation aircraft. The PIF control system is a unified approach combining computation delay accommodation, integral control, feedback control, feedforward control and filtering to yield altitude select and heading select autopilot functions. A command model is used to generate desired trajectories the aircraft follows. The command model has no effect on closed-loop stability, but benefically affects transient response performance.

The constant gain autopilots stabilize the aircraft throughout it's normal flight regime. Flight test results demonstrated shortcomings in all autopilots designed using only simulation results. Iterative autopilot tuning resulted in improved autopilots which performed well in the flight tests under a number of turbulence conditions. Modifications of the approach to use output feedback are being developed.

ACKNOWLEDGMENTS

Barry Nixon, the saftey pilot, and George Miller, both from Princeton University, participated in the Flight Tests. Joseph Old from Research Triangle Institute, aided the authors in flight control programming. This research was sponsored by the NASA Langley Research Center under Contract NAS1-16303.

REFERENCES

1. Larson, G. C., "The Future of 'Autopilots'", Business and Commercial Aviation, March 1981.

2. Downing, D. R., Bryant, W. H. and Stengel, R. F., "NASA/Princeton Digital Avionics Flight Test Facility", Proceedings of the 3rd Digital Avionics Systems Conference, Forth Worth, Texas, November 1979.

3. Downing, D. R., Bryant, W. H. and Ostroff, A. J., "Flight Test of a VTOL Digital Autoland Systme Along Complex Trajectories", Proceedings of the 1979 AIAA Guidance and Control Conference, Boulder, Colorado, August 1979.

4. Broussard, J. R., Berry, P. W. and Stengel, R. F., "Modern Digital Flight Control System Design for VTOL Aircraft", NASA CR-159019, March 1979.

5. Broussard, J. R. and O'Brien, M. J., "Feedforward Control to Track the Output of a Forced Model", IEEE Trans. Auto. Control, Vol. AC-25, August 1980, pp. 851-852.

6. Dorato, P. and Levis, A. H., "Optimal Linear Regulators: The Discrete-Time Case", IEEE Trans. Auto. Control, Vol. AC-16, No. 6, December 1971, pp. 613-160.

7. Broussard, J. R., "Design, Implementation and Flight Testing of PIF Autopilots for General Aviation Aircraft", Information & Control Systems, Inc. Report No. 681102, October 1981.

8. Suit, W., "Aerodynamic Parameters of the NAVION Airplane Extracted from Flight Data", NASA TN D-6643, March 1972.

9. Broussard, J. R., "PIGCGT - A PIF Autopilot Design Program for General Aviation Aircraft", Information & Control Systems, Inc. Report No. 681103, September 1981.

10. Roskam, J., Airplane Flight Dynamics and Automatic Flight Controls, Part I and II, Second Edition, Roskam Aviation Engineering Corp., Lawrence, Kansas, 1979.

11. Armstrong, E. S., ORACLS - A Design System for Linear Multivariable Control, Marcel-Dekher, Inc., New York, 1980.

12. McRuer, D. T. and Johnston, D. E., "Flight Control Systems Properties and Problems", NASA CR-2500, February 1975.

Table 1. Aircraft Data

Wing area	-	17.112 m^2	
Mean Aerodynamic Chord	-	1.74 m	
Wing Span	-	10.17 m	
Gross Mass	-	1540.6 kg	
I_X	-	1742.33 kg-m^2	
I_Y	-	3762.4 kg-m^2	
I_Z	-	4389.1 kg-m^2	
I_{XZ}	-	0.0	
Altitude	-	1524.0 m	
Velocity (true airspeed)	-	44.0 m/sec	
Flaps	-	20 deg	
$C_{X\alpha}$	1.37	C_{Yp}	0.0
$C_{Z\alpha}$	-4.86	C_{Yr}	0.0
$C_{Z\delta e}$	0.52	$C^*_{Y\delta r}$	-0.143
$C_{M\dot{\alpha}}$	-0.84	$C^*_{L\delta r}$	-0.023
$C_{M\alpha}$	-6.0	$C_{L\beta}$	-0.053
C_{Mq}	-16.4	C_{Lp}	-0.53
$C_{M\delta e}$	1.55	C_{Lr}	0.114
θ_o	0.105 rad	$C_{L\delta a}$	0.16
w_o	4.6 m/sec	$C_{N\beta}$	0.08
u_o	44.0 m/sec	C_{Np}	-0.147
α_o	0.105 rad	C_{Nr}	-0.12
C_{Xo}	0.0015	$C_{N\delta r}$	-0.0015
C_{Zo}	-0.75	$C_{N\delta a}$	0.075
C_{Zq}	-27.13	$C_{Y\beta}$	-0.74

* different from values in[8].

Table 2. Command Generator Control System Parameters

AUTOPILOT	EQUATION	PARAMETERS	VALUE	UNITS
HDG SEL	34	b_1	1.0	---
	34	b_2	2.0	---
	36	ϕ_{max}	0.209	rads
	37	ψ_e	0.157	rads
	38	$\dot{\phi}_{max}$	0.0873	rads/sec
	30	b	10.0	---
ALT SEL	34	b_1	0.8	---
	34	b_2	2.0	---
	36	$\dot{z}_{max}$	2.53	m/s
	37	z_e	6.0	m
	38	$\ddot{z}_{max}$	0.2286	m/s^2

Table 3. Autopilot Closed-Loop Eigenvalues

DYNAMIC MODE	OPEN LOOP			ALT SEL (LOWER θ WEIGHT)		
	ω_n, rad/sec	ξ, -	τ, sec	ω_n, rad/sec	ξ, -	τ, sec
SHORT PERIOD	3.0	0.78	---	3.07	0.77	---
PHUGOID	0.25	0.025	---	---	---	---
z	---	---	$-\infty$	---	---	---
$\delta_e - \theta$				1.12	0.81	---
$z - \int z$				0.36	0.80	---
V				---	---	24.3

DYNAMIC MODE	OPEN LOOP			ALT SEL (DESIGN)		
	ω_n, rad/sec	ξ, -	τ, sec	ω_n, rad/sec	ξ, -	τ, sec
SHORT PERIOD	3.0	0.78	---	3.07	0.69	---
PHUGOID	0.25	0.025	---	---	---	---
z	---	---	$-\infty$	---	---	---
$\delta_e - \theta$				1.58	0.99	---
$z - \int z$				0.25	0.77	---
V				---	---	24.2

DYNAMIC MODE	OPEN LOOP			HDG SEL		
	ω_n, rad/sec	ξ, -	τ, sec	ω_n, rad/sec	ξ, -	τ, sec
DUTCH ROLL	2.07	0.22	---	---	---	---
ROLL	---	---	0.16	---	---	0.16
SPIRAL	---	---	-31.0	---	---	---
HEADING	---	---	$-\infty$	---	---	---
DUTCH ROLL - δ_r				2.84	0.46	---
$\int\delta_r - v$				0.24	0.79	---
$\delta_a - \phi$				1.77	0.67	---
$\int\phi - \psi$				1.42	0.82	---

Table 4. Autopilot Gains

STATE*	FEEDBACK/FEEDFORWARD GAINS			
	ALT SEL ELEVATOR (DESIGN)	ALT SEL ELEVATOR (LOWER Θ WEIGHT)	HDG SEL AILERON	HDG SEL RUDDER
v_e	0.719	0.79	-	-
v_a	-	-	0.69	0.061
v_r	-	-	0.063	0.715
V	-0.025	-0.018	-	-
a_z	-0.021	-0.015	-	-
q	-0.428	-0.28	-	-
θ	-2.2	-1.48	-	-
z	0.0139	0.012	-	-
a_y	-	-	0.012	0.537
r	-	-	0.25	-2.0
p	-	-	-0.26	0.087
ϕ	-	-	-1.51	-0.44
ψ	-	-	0.50	-5.9
ξ_{long}	0.000176	0.000183	-	-
ξ_{lat1}	-	-	-0.014	0.032
ξ_{lat2}	-	-	0.028	0.013
u_{mlong}	-0.0491	-0.029	-	-
u_{mlat1}	-	-	1.15	1.28
u_{mlat2}	-	-	-1.19	-0.59

* units are radians and meters

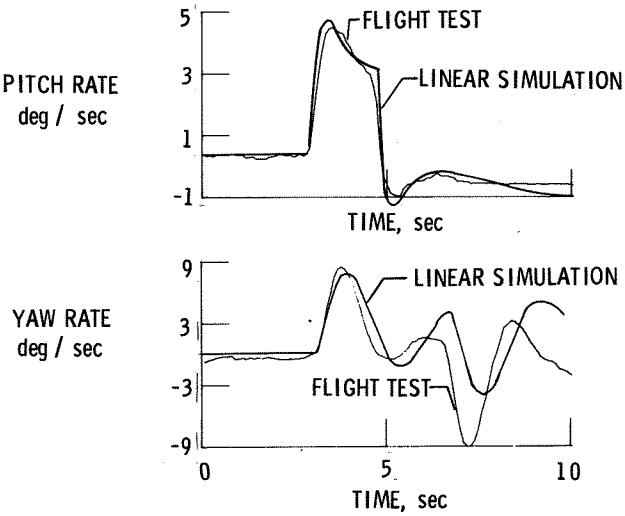

Figure 2. Comparison of Open-Loop Linear Model Response with Aircraft Response for a Step Command in Control Position

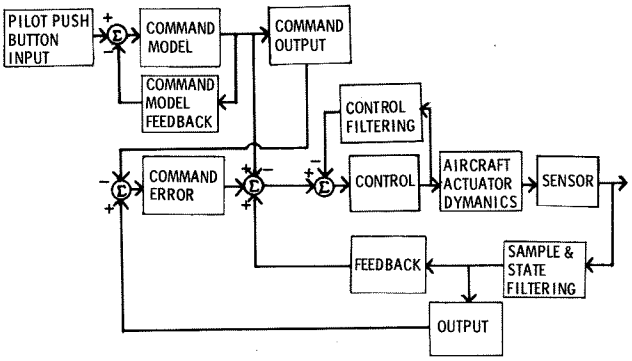

Figure 1. Basic PIF Control Law Block Diagram

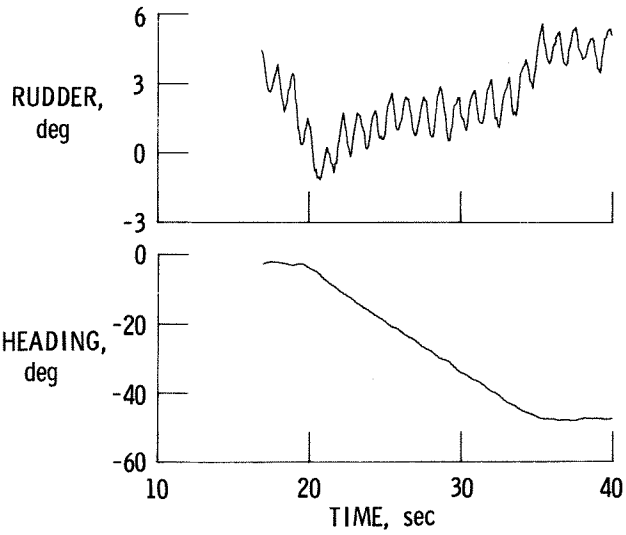

Figure 3. Heading Change with 0.01 sec Time Constant a_y Prefilter

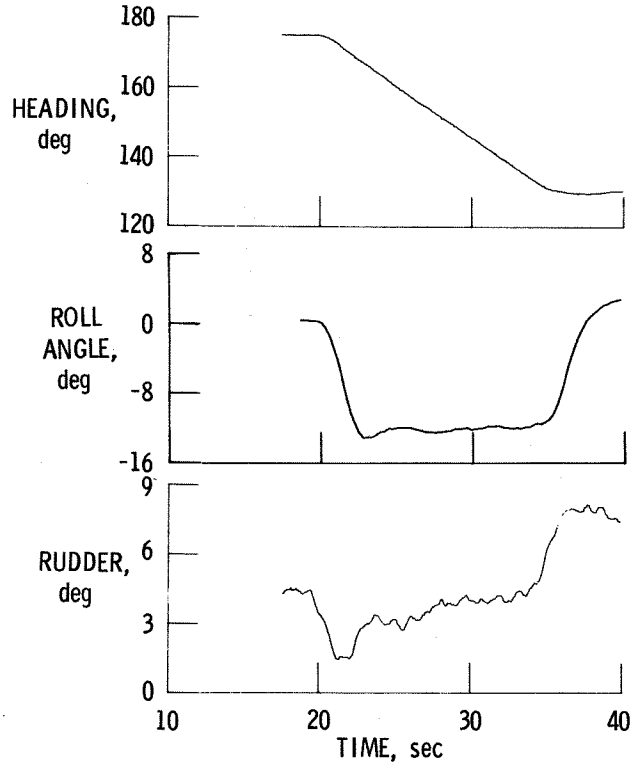

Figure 4. Heading Change with 0.1 sec Time Constant a_y Prefilter

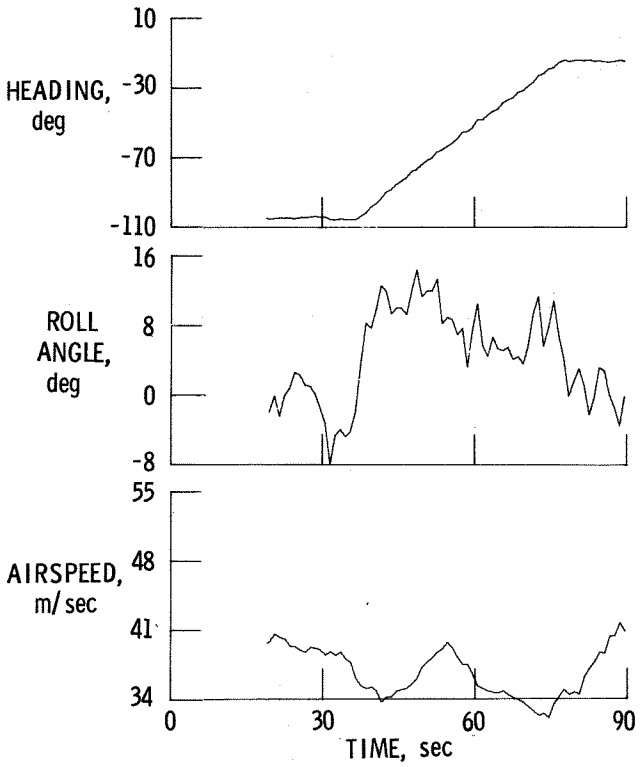

Figure 6. Heading Change in Heavy Turbulence

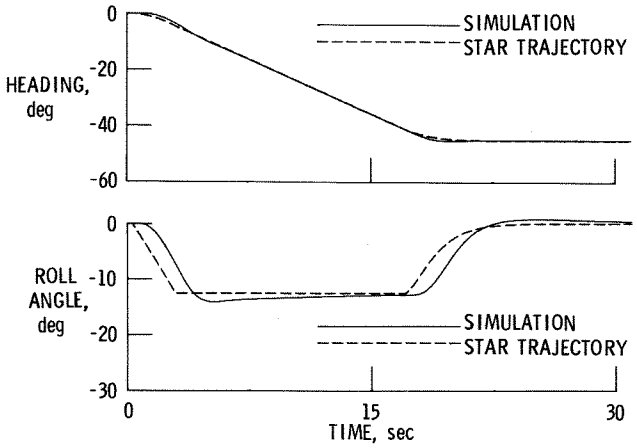

Figure 5. Simulation of Heading Change

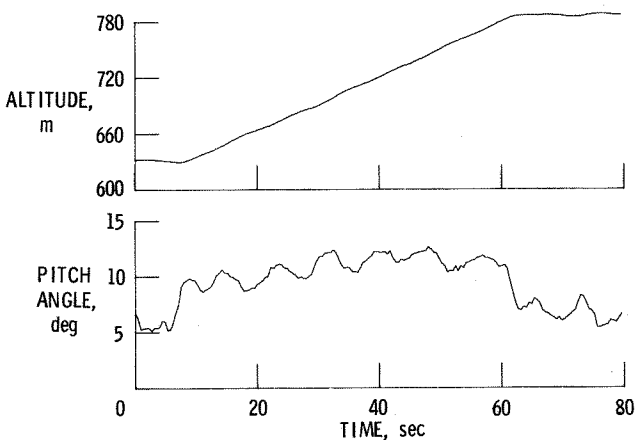

Figure 7. Altitude Change Using Low Pitch Weight Gain Set

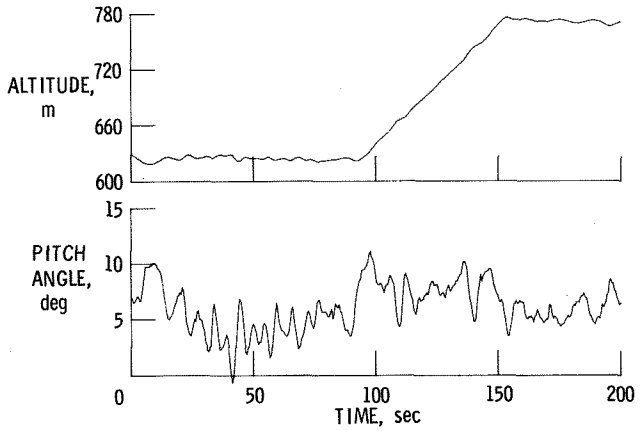

Figure 8. Altitude Change in Heavy Turbulence

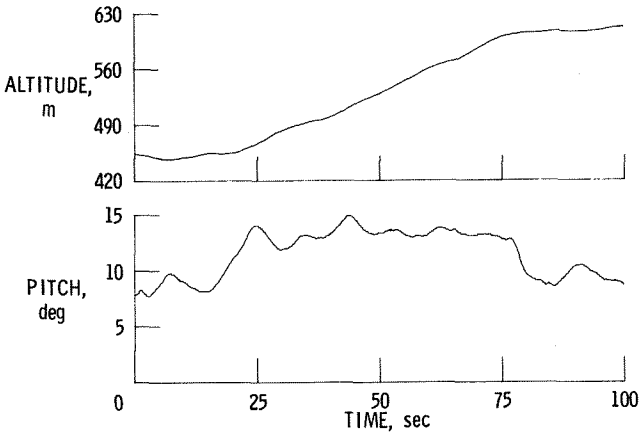

Figure 10. Altitude Change Using Design Gain Set

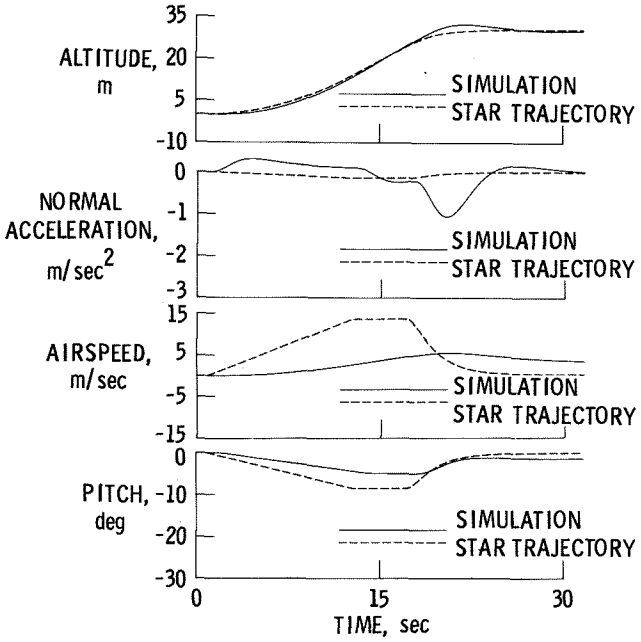

Figure 9. Simulation of Altitude Change